To show that the response is indeed from the polymer within the gap, we studied the I-V response as a function of photoexcitation with a Xe lamp (150 W). The I-V response for the polymer-filled nanowire becomes slightly more conductive upon Xe light exposure. During the backward scan, the device was irradiated with the Xe lamp starting at –0.1 V (red arrows in Fig. 2A), and a change in slope in the I-V response was observed. The transient conductance change between 1.1 nS in the dark to 1.6 nS when irradiated is consistent with an increase in charge-carrier density, which would be expected if the gap were filled with the p-type polypyrrole (*16*).

We report a novel lithographic process that allows one to generate designed gap structures on nanowire templates. The process is remarkably controllable, high-yielding, and easy to implement. It does not require sophisticated and expensive instrumentation and facilities, and it allows manipulation of an important class of structures that cannot be easily manipulated with conventional lithographic tools. Being able to make gap or notched structures with nanowires with OWL and relatively inexpensive instrumentation will facilitate the study of the electronic properties of nanomaterials and open avenues to the preparation of novel disk structures, which could be designed to have unusual optical properties as a function of gap and metal segment size [e.g., plasmon waveguides (*17*)].

References and Notes

1. B. D. Gates *et al.*, *Chem. Rev.* **105**, 1171 (2005).
2. M. A. Reed, C. Zhou, C. J. Muller, T. P. Burgin, J. M. Tour, *Science* **278**, 252 (1997).
3. J. Reichert *et al.*, *Phys. Rev. Lett.* **88**, 176804 (2002).
4. H. Park, A. K. L. Lim, A. P. Alivisatos, J. Park, P. L. McEuen, *Appl. Phys. Lett.* **75**, 301 (1999).
5. C. Z. Li, H. X. He, N. J. Tao, *Appl. Phys. Lett.* **77**, 3995 (2000).
6. J. Xiang *et al.*, *Angew. Chem. Int. Ed. Engl.* **44**, 1265 (2005).
7. C. R. Martin, *Science* **266**, 1961 (1994).
8. D. Routkevitch, T. Bigioni, M. Moskovits, J. M. Xu, *J. Phys. Chem.* **100**, 14037 (1996).
9. S. R. Nicewarner-Pena *et al.*, *Science* **294**, 137 (2001).
10. N. I. Kovtyukhova, T. E. Mallouk, *Chem. Eur. J.* **8**, 4354 (2002).
11. A. K. Salem, M. Chen, J. Hayden, K. W. Leong, P. C. Searson, *Nano Lett.* **4**, 1163 (2004).
12. S. Park, J.-H. Lim, S.-W. Chung, C. A. Mirkin, *Science* **303**, 348 (2004).
13. Materials and methods are available as supporting material on *Science* Online.
14. R. D. Piner, J. Zhu, F. Xu, S. Hong, C. A. Mirkin, *Science* **283**, 661 (1999).
15. D. S. Ginger, H. Zhang, C. A. Mirkin, *Angew. Chem. Int. Ed. Engl.* **43**, 30 (2004).
16. S. Park, S.-W. Chung, C. A. Mirkin, *J. Am. Chem. Soc.* **126**, 11772 (2004).
17. S. A. Maier *et al.*, *Nat. Mater.* **2**, 229 (2003).

18. C.A.M. acknowledges the U.S. Air Force Office of Scientific Research (AFOSR), Defense Advanced Research Projects Agency (DARPA), and NSF for support of this research.

Supporting Online Material
www.sciencemag.org/cgi/content/full/309/5731/113/DC1
Materials and Methods
Figs. S1 to S4

23 March 2005; accepted 9 May 2005
10.1126/science.1112666

Atlantic Ocean Forcing of North American and European Summer Climate

Rowan T. Sutton* and Daniel L. R. Hodson

Recent extreme events such as the devastating 2003 European summer heat wave raise important questions about the possible causes of any underlying trends, or low-frequency variations, in regional climates. Here, we present new evidence that basin-scale changes in the Atlantic Ocean, probably related to the thermohaline circulation, have been an important driver of multidecadal variations in the summertime climate of both North America and western Europe. Our findings advance understanding of past climate changes and also have implications for decadal climate predictions.

Instrumental records show that during the 19th and 20th centuries, there were marked variations on multidecadal time scales in the summertime climate of both North America (*1*–*4*) and western Europe (*5*). In the continental United States, there were significant variations in rainfall and drought frequency (*1*–*4*), and it has been suggested (*1*, *4*) that changes in the Atlantic Ocean, associated with a pattern of variation known as the Atlantic Multidecadal Oscillation (AMO) (*6*, *7*), were responsible. If confirmed, such a link would be important for climate predictions because the AMO is thought to be driven by the ocean's thermohaline circulation (*6*) and may be predictable (*8*, *9*). However, thus far the evidence for an Atlantic link is mainly circumstantial, being derived from observations and showing correlation rather than causality. Clarifying whether AMO-related changes in the Atlantic Ocean were indeed responsible for the observed variations in North American summer climate and whether, in addition, there were impacts on other regions is therefore an important challenge.

Figure 1 shows the time series and pattern of North Atlantic sea surface temperatures (SSTs) that characterize the AMO during the period 1871 to 2003 (*10*). There are AMO warm phases in the late 19th century and from 1931 to 1960; cool phases occur from 1905 to 1925 and from 1965 to 1990. The spatial pattern shows anomalies of the same sign over the whole North Atlantic, with the largest anomalies ($\sigma \sim 0.3$°C) found just east of Newfoundland.

Natural Environment Research Council Centres for Atmospheric Science, Centre for Global Atmospheric Modelling, Department of Meteorology, University of Reading, Post Office Box 243, Earley Gate, Reading RG6 6BB, UK.

*To whom correspondence should be addressed. E-mail: r.sutton@reading.ac.uk

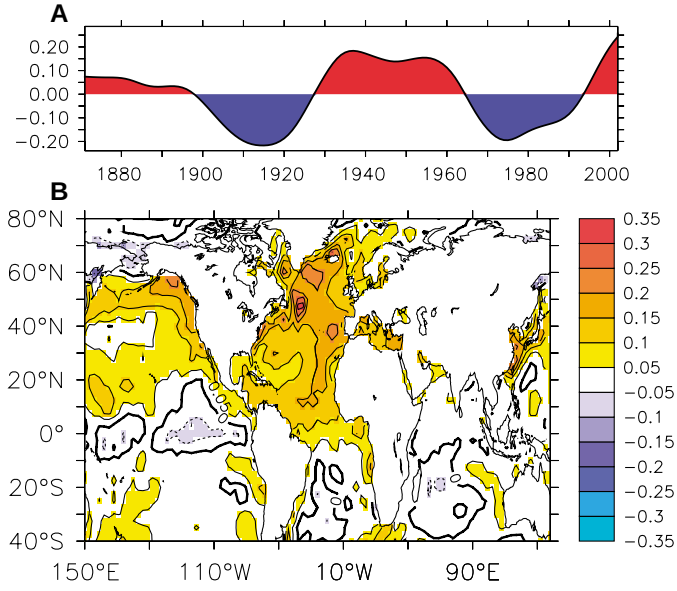

Fig. 1. (**A**) Index of the AMO, 1871 to 2003. The index was calculated by averaging annual mean SST observations (*29*) over the region 0°N to 60°N, 75°W to 7.5°W. The resulting time series was low-pass filtered with a 37-point Henderson filter and then detrended, also removing the long-term mean. The units on the vertical axis are °C. This index explains 53% of the variance in the detrended unfiltered index and is very similar to that shown in (*1*). (**B**) The spatial pattern of SST variations associated with the AMO index shown in (A). Shown are the regression coefficients (°C per SD) obtained by regressing the detrended SST data on a normalized (unit variance) version of the index.

To identify the climate variations associated with the AMO, we considered a simple composite difference of observational sea-level pressure (SLP), precipitation, and surface air temperature (SAT) data between the warm phase from 1931 to 1960 and the subsequent 30 years, 1961 to 1990, which were dominated by a cool phase of the AMO (Fig. 2, A to C). In the North Atlantic region, there are two prominent low-pressure anomalies, one centered over the southern United States (~60 Pa) and the other centered just west of the United Kingdom (peaking at ~150 Pa). The low-pressure anomaly over the southern United States is associated with precipitation reductions of up to 20% (0.1 to 0.3 mm/day), consistent with (*1*) and (*4*). Over western Europe, there is enhanced precipitation (0.1 to 0.3 mm/day, or 5% to 15% of the mean summer value). This multidecadal change in European precipitation has been previously documented (*5*) but has not been linked with the AMO. The SAT fields (Fig. 2C) show warm anomalies (0.25°C to 0.75°C) over the United States and also over central Europe. The precipitation fields (Fig. 2B) also show large positive anomalies in the Sahel region of North Africa, consistent with earlier work (*11*), and in the Caribbean.

A simple significance test (*12*) suggests that the major observed anomalies shown in Fig. 2 are unlikely to have arisen from internal fluctuations of the atmosphere. To investigate whether they arose in response to changes in the ocean, we first examined results from an ensemble of six simulations with an atmospheric general circulation model. These "C20" simulations were forced with historical global SST data for the period 1871 to 1999, and variations in the ensemble mean provide information about the ocean forcing of climate (*13*). Figure 2, D and E, shows the ensemble mean SLP and precipitation anomalies corresponding to the composite differences computed from observations. The SLP shows low-pressure anomalies centered over the southern United States and in the region of the United Kingdom that are in good agreement with the observations. The anomalies over the United States are very similar in magnitude to the observations (60 to 75 Pa), whereas the anomalies west of the United Kingdom are weaker in the model ensemble mean (~50 Pa) than in the observations (~150 Pa). The most likely reason for this discrepancy is a larger component of internal variability in the observations, a hypothesis supported by analysis of the ensemble spread (fig. S3).

The precipitation field (Fig. 2E) shows reduced precipitation over the United States and northern Mexico, and the magnitude of the anomalies (0.1 to 0.3 mm/day) is in agreement with the observations. Over western Europe, the model indicates enhanced precipitation consistent with the observations, but on the basis of our sample of six ensemble members, the anomalies are not statistically significant and are therefore not seen in the figure. The model shows large increases in precipitation in a tropical band stretching from the eastern Pacific, through the Caribbean and tropical Atlantic, to North Africa. The anomalies in the Caribbean and northern South America agree with the land observations in these regions, but the anomalies in the Sahel region are markedly weaker than is observed. This discrepancy might be a consequence of errors in the representation of land-surface feedbacks (*14*, *15*).

The results from the C20 simulations provide strong evidence that the major North Atlantic features identified in the observations arise in response to changes in the oceans. Results from similar experiments with other atmospheric models are consistent with this conclusion (*16*). However, because in each case the model was forced with global SST fields, these experiments do not clearly demonstrate the role of the Atlantic Ocean. To clarify the role of the Atlantic, we forced the model with an idealized AMO SST anomaly pattern, based on the North Atlantic part of Fig. 1B (see fig. S1). For these experiments, SST anomalies did not vary in time, but integrations of 10 or 20 years' duration were carried out to separate the ocean's influence from atmospheric internal variability (*12*).

Figure 2, F to H, shows the response to the AMO SST pattern. Over the Caribbean, central America, and the United States, the SLP and precipitation fields show excellent agreement with both the C20 simulations and the observations. The low-pressure anomalies in western Europe are also reproduced. Over the United Kingdom, there are positive precipitation anomalies, which were not seen in the C20 simulations but are in the observations, whereas precipitation anomalies over the Sahel are again weaker than observed (*17*). The SAT fields (Fig. 2H) show a prominent warm anomaly

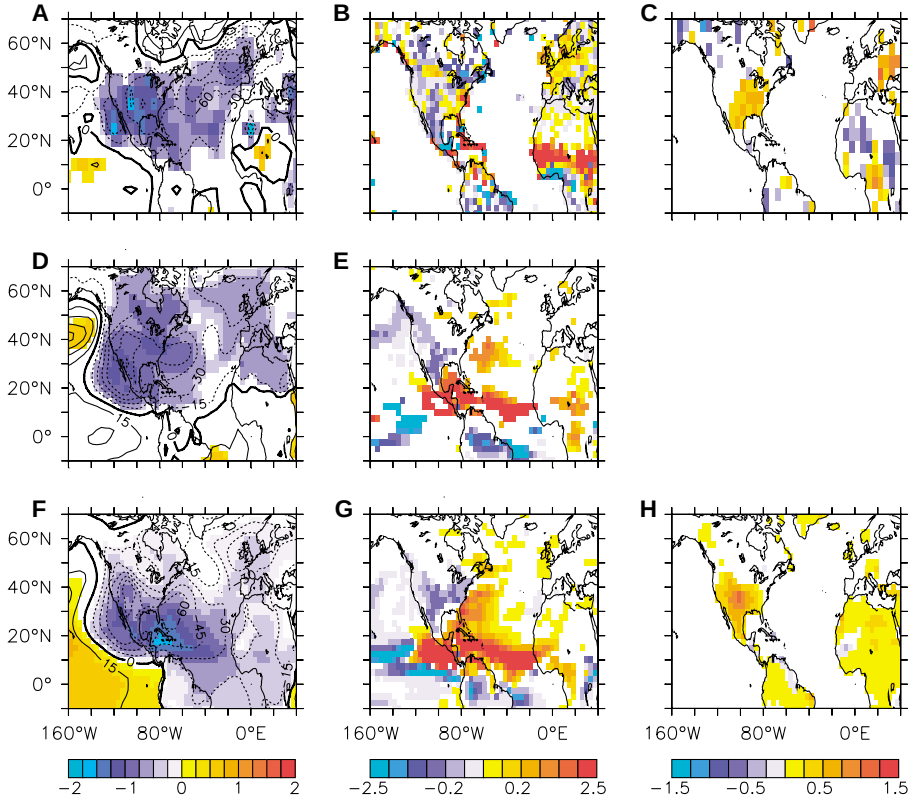

Fig. 2. Evidence of AMO impacts on boreal summer [June, July, and August (JJA)] climate. (**A** to **C**) Observed differences between the mean JJA conditions from 1931 to 1960 (a warm phase of the AMO) and the mean JJA conditions from 1961 to 1990 (a cold phase of the AMO). (A) Sea-level pressure. Contours are in Pa with an interval of 30 Pa; shading indicates signal-to-noise ratio (*12*). (B) Land precipitation (mm/day). (C) Land surface air temperature (°C). The scale for precipitation is nonlinear; the central range is (–0.5, 0.5). Values between (0.5,2.5) and (–2.5,–0.5) are each shaded with a single color. (**D** and **E**) As in (A) and (B), but computed from the ensemble mean of six simulations with the HadAM3 atmosphere model forced with observed SST data. In (D), the contour interval is 15 Pa. (**F** to **H**) As in (A) to (C), but showing differences between time means of simulations with the HadAM3 model forced with positive and negative signs of an idealized AMO SST pattern. (The pattern is based on the North Atlantic part of Fig. 1B and is shown exactly in fig. S1.) In (F), the contour interval is 15 Pa. All the values have been appropriately scaled to allow comparison with the other panels (*12*). In (A) and in (C) to (H), regions where anomalies are not significant at the 90% level are shaded white. In (E) and (G), precipitation values are shown over the sea as well as the land. Details of the model experiments and analyses are given in (*12*).

over the southern United States and Mexico, in agreement with the observations, and also show positive anomalies in western Europe. Overall, Fig. 2 provides compelling evidence that the AMO has indeed been responsible for marked changes in the regional atmospheric circulation and for associated anomalies in precipitation and surface temperature over the United States, southern Mexico, and, probably, western Europe.

The fact that the AMO SST experiments and the C20 simulations give such similar results suggests that, for the particular decadal change considered (1931 to 1960 compared with 1961 to 1990), the Atlantic Ocean was the dominant oceanic influence on summertime climate in the regions considered. To investigate the importance of the AMO over a longer period of time, we examined the correlation between the AMO SST index (Fig. 1A) and indices of SLP for the U.S. and U.K. regions (*12*). The SLP indices were computed both from the observations and from the C20 simulations. All the SLP indices are significantly anticorrelated with the AMO index (fig. S2). These results confirm that the AMO is an important influence on both regions, but they also suggest that other influences are important, especially for the U.S. region (for which the correlation with observed SLP is lowest). The much higher correlation between the AMO index and simulated U.S. SLP could suggest that these other influences [e.g., associated with changes in the Pacific Ocean (*3*)] are underestimated in the HadAM3 simulations.

To understand better the AMO influence, we performed two additional model experiments, using as forcing patterns the tropical part (0°N to 30°N) and the extratropical part (30°N to 70°N) of the AMO SST pattern (see fig. S1). The results (Fig. 3) indicate that AMO-related climate anomalies over the United States and Mexico were forced by tropical Atlantic SST anomalies, whereas those in the region of western Europe were primarily (but not exclusively) forced by SST anomalies in the extratropics. The low-pressure center over the southern United States may be a response to the anomalous latent heating of the atmosphere implied by the enhanced precipitation in the tropical Atlantic (*18*). The low-pressure center near the United Kingdom may be a downstream response to the largest positive SST anomalies east of Newfoundland (*19*, *20*). In Fig. 3, A and B, the impacts of the AMO are not restricted to the Atlantic basin but extend throughout the tropics. This finding supports suggestions (*21*, *22*) that the Atlantic Ocean may be an important driver of multidecadal climate variability on a global, as well as regional, scale.

Overall, our results provide strong evidence that during the 20th century the AMO had an important role in modulating boreal summer climate on multidecadal time scales. We have focused here on time mean anomalies, but some of the most important impacts are likely to be associated with changes in the frequency of extreme events. There is evidence that the frequency of U.S. droughts (*4*) and the frequency of European heat waves (*23*) are both sensitive to Atlantic SSTs.

The results also have implications for the interpretation of instrumental and proxy (*24*) climate records, which relies on understanding and quantifying how regional climate is related to large-scale drivers such as the AMO. Progress in understanding these drivers is especially important as studies that address the attribution of observed climate changes to anthropogenic causes give increasing attention to regional scales (*25*). Our results suggest, for example, that the change in phase of the AMO in the 1960s may have caused a cooling of U.S. and European summer climate; a further change in the AMO may have contributed to recent warming in these regions.

In addition, our results have implications for predicting the climate of the next few decades. In the absence of anthropogenic effects and assuming a period of 65 to 80 years (*1*, *26*), we should now be entering a warm phase of the AMO, as suggested by Fig. 1A. Our results would then suggest a forecast of decreased (relative to 1961 to 1990) summer precipitation (increasing drought frequency) and warmer temperatures in the United States together, possibly, with increased summer precipitation and temperatures in western Europe. In reality, anthropogenic effects on climate now appear to be important (*27*), so current and near future trends in North Atlantic regional climate may be shaped by a competition between the AMO and these anthropogenic effects. Moreover, these two influences may not add linearly. Models suggest that anthropogenic warming will lead to a slowdown of the Atlantic thermohaline circulation (*27*). If true of the real world, this could favor an earlier than expected shift toward the negative phase of the AMO, with a corresponding shift in the AMO influences on U.S. and European summer climate.

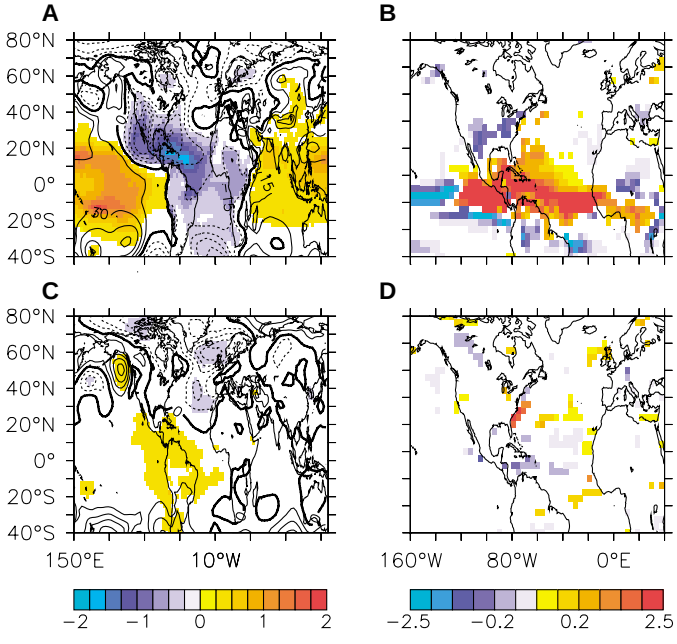

Fig. 3. Response of the HadAM3 model to tropical North Atlantic (TNA) and extratropical North Atlantic (XNA) parts of the AMO SST pattern. (**A** and **B**) Differences between time means of simulations with the HadAM3 model forced with positive and negative signs of the TNA SST pattern. (A) Sea-level pressure. Contours in Pa with an interval of 15 Pa; shading indicates signal-to-noise ratio (*12*). (B) Precipitation (mm/day); scale is nonlinear as described for Fig. 2. (**C** and **D**) As in (A) and (B), but for model simulations forced with the XNA SST pattern. The TNA and XNA SST patterns are shown in fig. S1. All values have been scaled to allow comparison with the Fig. 2 results. Regions where anomalies are not significant at the 90% level are shaded white.

References and Notes

1. D. Enfield, A. Mestas-Nunez, P. Trimble, *Geophys. Res. Lett.* **28**, 2077 (2001).
2. S. Schubert, M. Suarez, P. Pegion, R. Koster, J. Bachmeister, *J. Clim.* **17**, 485 (2004).
3. S. Schubert, M. Suarez, P. Pegion, R. Koster, J. Bachmeister, *Science* **303**, 1855 (2004).
4. G. McCabe, M. Palecki, J. Betancourt, *Proc. Natl. Acad. Sci. U.S.A.* **101**, 4136 (2004).
5. J. W. Hurrell, C. Folland, *Clivar Exchanges* **7**, 52 (2002).
6. T. Delworth, M. Mann, *Clim. Dyn.* **16**, 661 (2000).
7. R. Kerr, *Science* **288**, 1984 (2000).
8. S. Griffies, K. Bryan, *Science* **275**, 181 (1997).
9. M. Collins *et al.*, *Clivar Exchanges* **8**, 6 (2003).
10. Figure 1 is derived from annual mean data, but the AMO time series is extremely similar whether derived only from summer data or only from winter data. This finding indicates that air-sea interactions in summer are insufficient to erase from the summer mixed-layer memory of the AMO phase.
11. C. Folland, T. Palmer, D. Parker, *Nature* **320**, 602 (1986).
12. Materials and methods are available as supporting material on *Science* Online.
13. Individual ensemble members differed only with respect to the atmospheric initial conditions. To isolate the role of ocean changes, no time variation in radiatively active gases was included. For further details of the simulations, see (*12*). SAT fields from these simulations are unfortunately not available.
14. A. Giannini, R. Saravanan, P. Chang, *Science* **302**, 1027 (2003).
15. R. Koster *et al.*, *Science* **305**, 1138 (2004).
16. J. W. Hurrell, personal communication.
17. However, early individual basin experiments (*28*) with a different atmosphere model indicate that

SSTs in individual ocean basins may have less influence on Sahel rainfall than the tropics as a whole.
18. A. Gill, *Q. J. R. Meteorol. Soc.* **106**, 447 (1980).
19. Y. Kushnir *et al.*, *J. Clim.* **15**, 2233 (2002).
20. M. Rodwell, C. Folland, *Ann. Geophys.* **46**, 47 (2003).
21. B. Dong, R. Sutton, *Geophys. Res. Lett.* **29**, 1728 (2002).
22. R. Zhang, T. Delworth, *J. Clim.*, in press.
23. C. Cassou, L. Terray, A. Phillips, *J. Clim.*, in press.
24. S. Gray, L. Graumlich, J. Betancourt, G. Pederson, *Geophys. Res. Lett.* **31**, L12205 (2004); 10.1029/2004GL019932.
25. P. Stott, D. Stone, M. Allen, *Nature* **432**, 610 (2004).
26. M. Schlesinger, N. Ramankutty, *Nature* **367**, 723 (1994).
27. J. Houghton *et al.*, *Climate Change 2001: The Scientific Basis* (Cambridge Univ. Press, Cambridge, 2001).
28. C. Folland, J. Owen, M. Ward, A. Colman, *J. Forecasting* **10**, 21 (1991).
29. N. Rayner *et al.*, *J. Geophys. Res.* **108**, 4407; 10.1029/2002JD002670 (2003).
30. R.T.S. is supported by a Royal Society University Research Fellowship. D.L.R.H. is supported by the NERC Centres for Atmospheric Science. We are grateful to colleagues at the Met Office Hadley Centre for providing the HadISST and HadSLP data sets and results from the C20 global SST experiments. We thank J. Hurrell for valuable comments on the paper.

Supporting Online Material
www.sciencemag.org/cgi/content/full/309/5731/115/DC1
Materials and Methods
Figs. S1 to S3
References

6 January 2005; accepted 20 May 2005
10.1126/science.1109496

GRIP Deuterium Excess Reveals Rapid and Orbital-Scale Changes in Greenland Moisture Origin

V. Masson-Delmotte,[1]* J. Jouzel,[1] A. Landais,[1] M. Stievenard,[1] S. J. Johnsen,[2,3] J. W. C. White,[4] M. Werner,[5] A. Sveinbjornsdottir,[3] K. Fuhrer[6]

The Northern Hemisphere hydrological cycle is a key factor coupling ice sheets, ocean circulation, and polar amplification of climate change. Here we present a Northern Hemisphere deuterium excess profile covering one climatic cycle, constructed with the use of $\delta^{18}O$ and δD Greenland Ice Core Project (GRIP) records. Past changes in Greenland source and site temperatures are quantified with precipitation seasonality taken into account. The imprint of obliquity is evidenced in the site-to-source temperature gradient at orbital scale. At the millennial time scale, GRIP source temperature changes reflect southward shifts of the geographical locations of moisture sources during cold events, and these rapid shifts are associated with large-scale changes in atmospheric circulation.

The atmospheric water cycle plays a key role in climate change. At various time scales, changes in atmospheric moisture transport are intimately involved in key processes within the climate system, such as the growth of ice sheets or the freshwater budget of the ocean. Here we use an integrated tracer of the water cycle, the isotopic composition of the ice preserved in Greenland, to decipher changes in Greenland moisture origin over the last glacial cycle.

Water stable isotopes ratios ($\delta^{18}O$ or δD) from polar ice cores are commonly used as past temperature proxies (*1*, *2*), a function made possible by the progressive distillation of heavy water isotopes when air masses cool toward polar regions (*3*–*5*). Comparison of Greenland temperature (T_{site}) values derived from ice $\delta^{18}O$ using the observed modern spatial gradient with alternative paleothermometry methods yields a systematic underestimation of past surface annual mean temperature changes, both at glacial-interglacial (*6*–*8*) and rapid-events time scales (*9*–*13*). Such discrepancies are thought to arise from variability in the Northern Hemisphere hydrological cycle, either from changes in moisture source areas (*14*) or from changes in the seasonality of precipitation (*15*, *16*).

We used high-precision continuous water stable isotope measurements made on the GRIP ice core (table S1) to calculate a Northern Hemisphere deuterium excess $d = [\delta D - (8 \times \delta^{18}O)]$ profile covering one climatic cycle (*17*). This deuterium excess record, together with a method to account for changes in precipitation seasonality, was then used to quantify past changes in Greenland moisture source temperature.

Figure 1 shows both $\delta^{18}O$ and deuterium excess profiles for the last ~100,000 years (i.e., excluding the lowest part of the profiles characterized by ice flow disturbances) (*18*). The excess profile reveals well-defined features at glacial-interglacial time scales, with a 5 per mil (‰) increase during the last climatic transition (*5*), as well as for Dansgaard-Oeschger (D/O) events characterized by large (up to 5‰) excess changes, in antiphase with $\delta^{18}O$ changes. Similar rapid excess changes are also recorded in the North Greenland Ice Core Project (NorthGRIP) ice core for D/O events 18 to 20 (*13*). Such deuterium-excess variations essentially result from the fact that, with respect to equilibrium processes, kinetic isotopic effects play a much larger relative role for $\delta^{18}O$ than for δD. In turn, deuterium excess in polar snow, d_{snow}, is largely driven by nonequilibrium processes (i.e., evaporation at the ocean surface and condensation of water vapor when snow forms). Deuterium excess in water vapor over the ocean is mainly influenced by sea surface isotopic composition, sea surface temperature (SST), source temperature (T_{source}), and relative humidity. This imprint of oceanic conditions (here considered only in terms of T_{source}) in the moisture source areas is largely preserved in the deuterium excess signal recorded in polar snow (*19*). In turn, whereas δ_{snow} ($\delta^{18}O$ or δD) depends primarily on local temperature T_{site} and to a lesser degree on T_{source}, one can show that the opposite is true for d_{snow} (*20*, *21*).

Combining $\delta^{18}O$ and deuterium excess profiles allows us to estimate both T_{site} and T_{source}. This dual approach, based on the inversion (*22*) of a dynamically simple isotopic model (*23*), is now used for interpreting isotopic measurements performed on Antarctic cores (*24*–*26*). Although useful for the last millennium and for the Holocene in Greenland (*20*, *27*), this methodology leads to unrealistic results when applied directly to the long-term GRIP data (*21*). We show here that this difficulty can be overcome if this inversion accounts for the seasonality of snow precipitation, as suggested by general circulation model simulations. This allows us to interpret the $\delta^{18}O$ or δD GRIP data in terms of T_{site} and T_{source} changes in a consistent way, both for glacial-interglacial changes and for D/O events, thus providing high-resolution information on the source conditions and the reorganizations of the water cycle during slow and rapid climatic changes.

Seasonal characteristics are relatively well known for central Greenland's present-day climate. Field observations suggest a year-

[1]IPSL/Laboratoire des Sciences du Climat et de l'Environnement (LSCE), UMR CEA-CNRS, CEA Saclay, 91191 Gif-sur-Yvette, France. [2]Department of Geophysics, Juliane Maries Vej 30, University of Copenhagen, DK-2100 Copenhagen, Denmark. [3]Science Institute, University of Iceland, Dunhaga 3, Reykjavik 107, Iceland. [4]Institute of Arctic and Alpine Research Institute and Department of Geological Sciences, Campus Box 450, University of Colorado, Boulder, CO 80309, USA. [5]Max Planck Institute for Biogeochemistry, Postbox 10 01 64, D-07701 Jena, Germany. [6]Physics Institute, University of Bern, Sidlerstrasse 5, CH-3012 Bern, Switzerland.

*To whom correspondence should be addressed. E-mail: valerie.masson@cea.fr